ACS APPLIED MATERIALS & INTERFACES

Research Article

Cite This: ACS Appl. Mater. Interfaces 2019, 11, 33465−33477

www.acsami.org

Influence of Water on Structure, Dynamics, and Electrostatics of Hydrophilic and Hydrophobic Ionic Liquids in Charged and Hydrophilic Confinement between Mica Surfaces

Mengwei Han and Rosa M. Espinosa-Marzal*

University of Illinois at Urbana−Champaign, 205 North Matthews Avenue, Urbana, Illinois 61801, United States

Supporting Information

ABSTRACT: Water is ubiquitous in the environment and is the origin for operational constraints in ionic-liquid based electrolytes for supercapacitors. In this study, the influence of water on the interfacial behavior of hydrophilic (1-ethyl-3-methylimidazolium ethylsulfate, abbr. [EMIM][$EtSO_4$]) and hydrophobic (1-ethyl-3-methylimidazolium tris(pentafluoroethyl)trifluorophosphate and 1-ethyl-3-methylimidazolium bis(trifluoromethylsulfonyl)imide, abbr. [EMIM][FAP] and [EMIM][TFSI], respectively) ionic liquids (ILs) confined between mica surfaces was investigated at separations precisely modulated by a surface force apparatus and at controlled relative humidity between 0% and 50% RH. Diffusion experiments revealed that water spontaneously invades the nanoconfined ILs above a certain humidity threshold and that the confined hydrophobic IL is completely replaced by water at sufficiently high environmental humidity (~45% here) as a result of surface-induced phase separation. This behavior is expected to be universal for other ILs that are not fully miscible with water when they are confined in hydrophilic nanopores of a few nanometers in width. The effect of environmental humidity on interfacial structure, dynamics, and electrostatics was studied via dynamic force measurements. In the dry state, several layers of ions are immobilized on the mica surface, and the effective viscosity increases by up to 2 orders of magnitude with a decrease in film thickness from ~10 to ~3 nm. Based on recent work, it is proposed that nanoconfinement enhances the anion−cation association in highly concentrated electrolytes, thereby justifying the loss of fluidity of the ILs. When phase separation is excluded, water is intercalated in the layered structure of the three ILs, and it leads to a change of the layer thickness compared to the dry state. Furthermore, our results reveal that interfacial water prevents ions from being immobilized on the surface and facilitates the outflow of both hydrophilic and hydrophobic ILs by reducing their effective viscosity in the order [EMIM][FAP] < [EMIM][TFSI] < [EMIM][$EtSO_4$]. The underlying mechanisms are evaluated by considering the roles of water in enhancing ion dissociation through screening of electrostatic interactions and solvation of the selected ILs to different extents. The discussed experimental observations support the recent discoveries made by molecular dynamic simulations and neutron scattering studies that using hydrophilic ILs coupled with water as cosolvent could lead to the enhanced power density of IL-based supercapacitors, and therefore, that water-in-(hydrophilic) ILs is a direction worth exploring as electrolytes for supercapacitors.

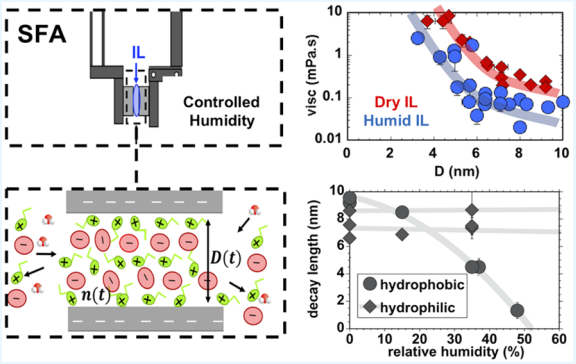

KEYWORDS: *ionic liquids, water, hydrophilic nanoconfinement, interfacial dynamics, interfacial structure*

1. INTRODUCTION

Next-generation supercapacitors promise a large energy storage density with high power output, and long cycling lifetimes through the formation of an electrical double layer (EDL) near the electrode's surface.[1,2] State-of-the-art supercapacitors use flammable and volatile organic electrolytes to achieve larger voltage windows than aqueous electrolytes.[3] Ionic liquids (ILs) are considered well-suited electrolyte substitutes because of their high charge density, thermal stability, wide electrochemical stability window, and nonvolatility, which reduces environmental exposure and prevents the risk of explosion.[4] Coupled with electrodes with large surface areas, ILs could theoretically increase the stored charge at the solid−liquid interface while reducing safety risks, however, at the expense of reduced conductance due to their high viscosity. The high viscosity of ILs has been linked to reduced electrical conductivity and capacitance, poor wetting of porous electrodes, and lower power density of the device.[5,6]

Simulations[7] and experimental studies[8] both indicate that the transport of IL ions in the nanometer-sized pores of the electrodes can be slowed down by over 2 orders of magnitude compared to their unconfined motion. Surface force measure-

Received: June 21, 2019
Accepted: August 13, 2019
Published: August 13, 2019

DOI: 10.1021/acsami.9b10923
ACS Appl. Mater. Interfaces 2019, 11, 33465−33477

ments (see, e.g., ref 9 in refs therein) agree that ILs retain their bulk viscosity in films thicker than ∼10−20 nm, while the viscosity of the confined liquid increases by 1−3 orders of magnitude as the liquid is further confined from ∼5−20 to ∼1−3 nm. In the context of nonpolar solvents, this has been classically associated with the constrained motion of the liquid molecules imposed by the confining wall and the interactions with the solid surface.[10] However, because ILs are highly concentrated electrolytes, viscous−electric coupling phenomena during flow along the charged walls are possible. In this context, the shift of the slip plane away from the surface has been associated with the strong adsorption of counterions to charged[11] and biased surfaces.[12]

Various solutions have been proposed to reduce viscosity, including mixing ILs with aprotic cosolvents.[13] Our measurements with a surface force apparatus have shown that the squeeze-out of hydrophilic and hydrophobic ILs (1-ethyl-3-methylimidazolium ethylsulfate [EMIM][$EtSO_4$] and 1-ethyl-3-methylimidazolium tris(pentafluoroethyl)-trifluorophosphate [EMIM][FAP], respectively) sandwiched between mica surfaces is facilitated in the presence of water.[14,15] MD simulations[16] revealed for another hydrophobic IL that water mostly adsorbs on the mica surface, thereby displacing the imidazolium cations, which is accompanied by a change of the slippage plane from the interior of the film to the mica surface. This shift facilitates the squeeze-out of ions observed in experiments. In another study using carbide-derived carbon electrodes,[17] it was observed that water in 1-butyl-3-methylimidazolium bis(trifluoromethylsulfonyl)imide ([BMIM][TFSI]), a hydrophobic IL, increased both the power density and the capacitance. Here, it was also concluded that water molecules displaced ions from the pore surface, which improved the diffusivity of the displaced cations. On the other hand, water absorption by ILs may compromise the performance of supercapacitors, since water may adsorb on the electrode surfaces, reduce the IL voltage window, and contribute to the degration of the electrode material and to leakage of currents.[18] Based on molecular dynamics simulations and electrochemical cyclic voltammetry, it has been proposed more recently that hydrophilic ILs may be effective in mitigating electrosorption of water, and thereby in preventing electrolysis.[19] This could augment the voltage window that hinders the application of water-in-IL electrolytes to date. Based on this, water-in-(hydrophilic) ILs appear as a strategy to both assist ion transport and alleviate operational constraints related to the use of supercapacitors in dry environments or *in vacuo*.

Here, we have investigated the absorption of water by hydrophilic and hydrophobic ILs confined between hydrophilic mica surfaces at distances smaller than ∼10 nm and its effect on the squeeze-out of the ILs through this confined geometry. The insight provided in this work will help guide the design of water-in-IL electrolytes for energy storage.

2. EXPERIMENTAL METHODS

2.1. Surface Forces Apparatus. Diffusion and dynamic force measurements were carried out with a surface force apparatus (SFA) using mica as the confining surface in a cell with controlled relative humidity. A number of improvements for thermal and mechanical stability and resolution have been implemented in our SFA, which are detailed elsewhere.[20] For the sample preparation, ruby mica of optical grade #1 (S&J Trading Inc., NY) was manually cleaved to 2−3-μm-thick pieces in a class-100 laminar-flow hood and cut into 1 cm by 1 cm pieces. The mica sheets were laid on a backing sheet and a silver layer of 40 nm was deposited on the back side under vacuum (2×10^{-6} mbar) with an e-beam evaporator. Two back-silvered mica sheets of equal thickness were then glued onto cylindrical glass lenses with a radius of 2 cm using epoxy glue (EPON-1004, Shell Chemicals). The lenses were immediately mounted onto the SFA and equilibrated in a dry nitrogen atmosphere. After equilibration, the surfaces were slowly (1 nm/s) brought into mica−mica contact to determine the mica thickness in the dry atmosphere. The mechanical drift of our instrument over a period of 8 h is smaller than 0.2 nm.

In SFA measurements, a beam of white light passes through the semitransparent system composed of glass lenses, back-silvered mica surfaces, and the sandwiched ionic liquid, and it experiences multiple reflections at each optical interface. A prism splits the transmitted light into fringes of equal chromatic order (FECO), which are detected by a spectrometer and numerically analyzed by fast spectral correlation.[20] This numerical algorithmic simultaneously provides the distance at the point of closest approach (surface separation, D) with a precision of 25 pm and the refractive index of the sandwiched liquid (n) in real-time. The error in the measurement of the refractive index at surface separations between 1 and 3 nm is $\pm$0.02, and it increases dramatically at separations smaller than 1 nm.[20]

The relative humidity was measured with a humidity sensor (SHT75 humidity sensor, Newark, IL) inside the SFA cell (36 mm × 19 mm × 32 mm). The sensor was positioned approximately 1 cm above the mica surfaces. The cell was purged with a gentle flow of gas composed of a mixture of ultrahigh-purity dry nitrogen gas and ultrahigh-purity nitrogen saturated with Millipore water. The relative humidity was measured every 3 s and the flow rate of the two streams was tuned to maintain the humidity at the desired level. The initial tuning process took ∼1−5 min, during which a slight overshoot of humidity was possible for a very short period of time. The experiments were conducted at 0% RH (dry nitrogen), 15 ± 2% RH, 35 ± 2% RH, and 48 ± 3% RH.

2.2. Materials. Three ILs with the same cation were selected for these studies: one hydrophilic IL, [EMIM][$EtSO_4$], and two hydrophobic ILs, [EMIM][FAP] and [EMIM][TFSI]; see the molecular structures of the ions in Figure S1. A volume of 500 μL was dried under vacuum at 50 °C for 48 h before use. A volume of ∼200 μL was injected in the space between the mica surfaces under a continuous flow of dry N_2. In our SFA, the glass lenses with the liquid are located in the vertical position, so that an unknown amount of excess liquid is often lost by gravity. The spring constant used for the experiments was 2364 ± 60 N/m for [EMIM][TFSI] and [EMIM][$EtSO_4$] and 1920 ± 81 N/m for [EMIM][FAP] and [EMIM][$EtSO_4$]. The water content was gravimetrically measured by equilibrating ∼200 μL of each IL at the selected RHs in airtight chambers in separate experiments. The humidity inside the chambers was buffered by saturated aqueous solutions of LiCl at 12−15% RH, $MgCl_2$ at 33% RH, and K_2CO_3 at 44% RH.[21] There is a small difference between the selected RHs in the gravimetric experiments and the average RHs in the SFA experiments. However, this difference does not impair the conclusions of this work.

2.3. Methods. Two types of experiments were conducted with the SFA. In "diffusion" measurements, the ionic liquid was initially equilibrated with the nitrogen atmosphere ($RH_1 = 0$), after which the surfaces approached at a constant velocity of 0.3 nm/s to a separation (D) of 3.7 ± 0.5 nm. Once the system equilibrated, the humidity was varied to the next level (RH_2) and the change of the film thickness and of the refractive index was recorded with time at a rate of at least 3 Hz. These measurements were named "diffusion" experiments because the observed phenomena were induced by the diffusion of water from the gaseous environment into the liquid. After a maximum of 8 h, the surfaces were separated to a distance larger than 1 μm, and the humidity was maintained constant at RH_2 for at least 12 h before "dynamic force" measurements were started. Here, one of the lenses was driven by a piezometric actuator at constant velocity of 0.3 ± 0.08 nm/s and the force acting between the two surfaces was determined by converting the deflection of the spring to a force using Hooke's law with the known spring constant. Then, diffusion measurements were carried out again, so the surfaces approached to 3.7 ± 0.5 nm, the

DOI: 10.1021/acsami.9b10923
ACS Appl. Mater. Interfaces 2019, 11, 33465−33477

Table 1. Water Uptake (in Mole Ratio) By the Selected ILs at 0%, 15%, 35%, and 48% RH, as Well as Bulk Viscosity (η_0), Density (ρ), and Refractive Index (n) of [EMIM][$EtSO_4$] as a Function of the Water Content at 25 °C[a]

	[EMIM][$EtSO_4$]				[EMIM][TFSI]	[EMIM][FAP]
RH (%)	Water:IL	η_0 (mPa.s)	ρ (g/cm^3)	n (−)	Water:IL	Water:IL
0	0	116	1.238	1.484 ± 0.002	0	0
15	0.23 ± 0.03	79	1.233	1.475 ± 0.002	0.03 ± 0.02	0.03 ± 0.01
35	1.51 ± 0.01	58	1.213	1.466 ± 0.002	0.13 ± 0.02	0.08 ± 0.05
48	2.43 ± 0.02	33	1.197	1.450 ± 0.002	0.15 ± 0.03	0.09 ± 0.03

[a]The viscosity and density were taken from ref 29, and the refractive index was measured with our SFA.

humidity was either increased or decreased to the next level (RH_3) and the sequence was repeated. We investigated the following RH sequences: from 0% to 15% RH, from 15% to 35% RH, from 35% to 48% RH, from 0% and 15% to 48% RH as well as from 48% to 0% RH.

2.4. Analysis of Dynamic Force Measurements. To model the drainage of the ILs in dynamic force experiments, the same method was applied as in our previous study of *vacuum-dried* ILs.[11] Assuming linear force superposition, the measured spring force (F) gives the sum of surface forces (F_s) and viscous (hydrodynamic) drag (F_{visc})

$$F = F_s + F_{visc} = F_{el} + F_{vdW} + F_{solv} + F_{visc} \quad (1)$$

where F_{el} refers to the electrostatic interaction between charged mica surfaces; F_{vdW} is the van der Waals force; F_{solv} gives the solvation force; F_{visc} is the viscous drag due to the motion of the surface in the IL. The spring force F is calculated from the deflection of the spring via the Hooke's law

$$F = k(\Delta D - \Delta M) = k[D(t) - D_0 + Vt] \quad (2)$$

k being the spring constant and $(\Delta D - \Delta M)$ the deflection on the spring; ΔD is calculated as the change of the measured surface separation at any time $D(t)$ and the initial separation (D_0), at which the total force is negligible; ΔM is the distance traveled by the piezometric actuator over a time t at the constant velocity V.

Static surface force measurements have revealed the action of electrostatic forces in ILs with a decay length of ∼10 nm, much longer than expected from the Debye−Hückel theory.[22] The electrostatic force in ILs (F_{el}) has been shown to exponentially decay with surface separation

$$F_{el} = R{\cdot}B{\cdot}\exp\left(-\frac{D}{\lambda_s}\right) \quad (3)$$

where R is the radius of the two surfaces; B is an empirical prefactor that might be related to the surface potential and the screening length, like in the classical Debye−Hückel theory; and λ_s is the screening length of the electrostatic interactions. The van der Waals force is given by

$$F_{vdW} = -\frac{R{\cdot}A}{6D^2} \quad (4)$$

with A being the Hamaker constant, which can be determined using the Liftshitz theory;[23] the dielectric constants of the ILs used for this calculation can be found in Table S1. For liquids that arrange as molecular layers at solid−liquid interfaces, like ILs do,[24] the solvation force has been described by an oscillatory force superposed to an exponentially decaying force[25]

$$F_{solv} = -R{\cdot}C{\cdot}\cos\left(\frac{2\pi D}{\lambda_1}\right)\exp\left(-\frac{D}{\lambda_2}\right) \quad (5)$$

where C is an empirical prefactor, λ_2 is the decay length of the exponential component, and λ_1 is the periodicity of the oscillatory profile, which is equal to the thickness of the molecular layers.

The viscous force F_{visc} is modeled using Reynold's theory of lubrication, taking into account that the geometry provided by the two cylindrical SFA lenses (of radius R) is equivalent to a sphere with a radius R approaching a flat plate. The drag force applied on the approaching surface is thus given by[25]

$$F_{visc} = -\frac{6\pi R^2\eta}{D - 2D_s}\frac{dD}{dt} \quad (6)$$

where η is the viscosity of the confined fluid; D_s is the thickness of the firmly adsorbed layer of ions that remains immobile during drainage of the liquid. D_s is called "stick length" to differentiate it from the slip length; note that we called it "stop" length before.[11] To ensure that the sphere-plane geometry is maintained, the model is limited to normalized forces (F/R) smaller than ∼20 mN/m.

Substituting eqs 2−6 into eq 1 yields

$$k[D(t) - D_0 + Vt] = -\frac{6\pi R^2\eta}{D - 2D_s}\frac{dD}{dt} + R{\cdot}B{\cdot}\exp\left(-\frac{D}{\lambda_s}\right) - \frac{R{\cdot}A}{6D^2} - R{\cdot}C{\cdot}\cos\left(\frac{2\pi D}{\lambda_1}\right)\exp\left(-\frac{D}{\lambda_2}\right) \quad (7)$$

At separations $D \gtrsim 100$ nm, the surface force is negligible, and the hydrodynamic drag dictates the liquid drainage, so $F \sim F_{vis}$. Here, the approach velocity (V) is precisely adjusted to fit the data at very large separations (∼1 μm), while satisfactory fits are obtained by setting η equal to the bulk viscosity of the IL (η_0). At 100 nm > D > 10 nm, the force experienced by the spring is balanced by both the hydrodynamic force and the long-range electrostatic force because the solvation force and the van der Waals force are negligible. This yields a simplified force balance

$$k[D(t) - D_0 + Vt] = -\frac{6\pi R^2\eta}{D - 2D_s}\frac{dD}{dt} + R{\cdot}B{\cdot}\exp\left(-\frac{D}{\lambda_s}\right) \quad (8)$$

which is numerically integrated using the Runge−Kutta method with a sufficiently small time step to ensure convergence. The integration provides the equation of motion, i.e., an expression for $D(t)$, while the spring force $F(D)$ is calculated according to eq 2. The fitting parameters are B, λ_s, η, and D_s. We note that D_s mainly influences the range $D \lesssim 30$ nm at the selected approach velocity ($V \sim 0.3$ nm/s), while the onset of the electrostatic interaction occurs at larger separations, which enables decoupling of electrostatic and viscous forces.

At separations smaller than ∼10 nm, van der Waals and solvation forces cannot be neglected so that eq 7 is numerically integrated following the same approach as described above to obtain an expression for $D(t)$ and for the dynamic force $F(t)$. The van de Waals force can be calculated for each IL in equilibrium with humid environment considering the change of the permittivity calculated by the mixing rules[26] and with the measured refractive index. The unknown parameters (D_s, η, C, λ_1, and λ_2) are obtained via the fit of the equation of motion $D(t)$ and the spring force $F(D)$ to the experimental data, which is an iterative process.

3. RESULTS

The water uptake by the ILs was gravimetrically measured at the selected environment humidities, and it is shown in Table 1. In the following paragraphs, we use the term "IL" to refer to the liquid as a whole, while "ions" and "ion pairs" are used

DOI: 10.1021/acsami.9b10923
ACS Appl. Mater. Interfaces 2019, 11, 33465−33477

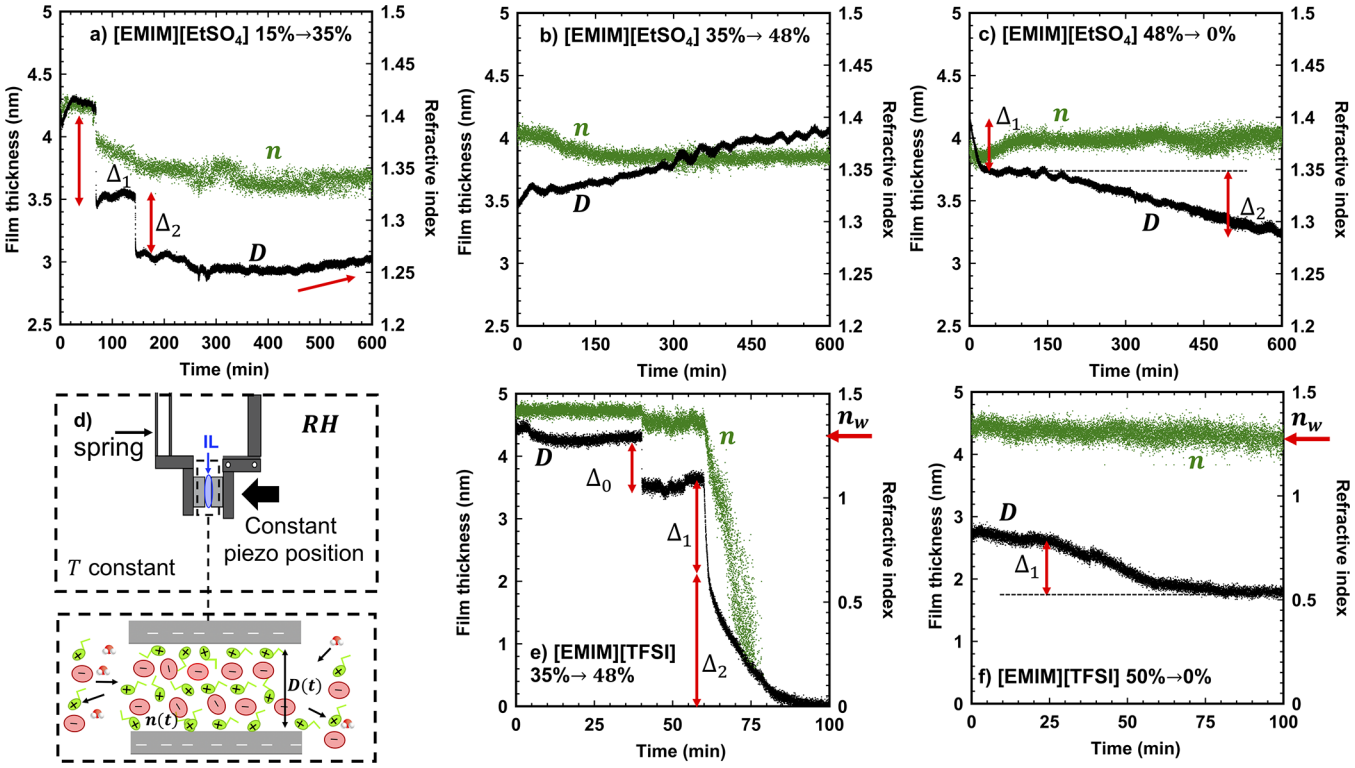

Figure 1. Representative measurements of film thickness (D) and refractive index (n) for (a–c) [EMIM][$EtSO_4$] and (e,f) [EMIM][TFSI] upon changes in environmental humidity. (d) Experimental setup for diffusion experiments carried out with an SFA. Water molecules and ions diffuse into and out of the confined film when subjected to changes in relative humidity at a constant temperature of 25 °C. The induced change of the surface force causes the cantilever to deflect so that the surface moves to a new equilibrium position.

when addressing the molecular-level behavior. Due to the small water uptake by [EMIM][TFSI] and [EMIM][FAP], their viscosity and density were assumed to remain constant in the range of investigated RHs (32 mPa.s and 1.52 g/cm^3 at 25 °C for [EMIM][TFSI][27] and 71 mPa.s and 1.71 g/cm^3 at 22 °C for [EMIM][FAP],[28] respectively), whereas the viscosity of [EMIM][$EtSO_4$] (η_0) and its density were obtained as a function of the water content at 25 °C using the data in ref 29 and are given in Table 1, as well.

3.1. Diffusion Experiments by SFA. The vacuum-dried IL was placed between the mica surfaces and equilibrated with a dry N_2 atmosphere. One of the two glass lenses was slowly moved toward the other to a surface separation of ~3.7 ± 0.5 nm. The relative humidity (RH) was then varied, and the change of film thickness and refractive index was measured in real time. The change of water content in the confined IL is expected to cause a change of short-range interactions between the confined molecules and the confined molecules and the surface, and thereby a change of the surface force F_s. For instance, a decrease in repulsion would decrease the deflection of the spring and bring the surfaces to a closer separation until a new equilibrium would be achieved. In addition to this, the change in composition of the confined film yields a change in refractive index, and the volume fraction of water (ϕ) can be roughly estimated according to[30]

$$n(t) = n_{IL} - \phi(n_{IL} - n_{water}) \quad (9)$$

where $n(t)$ is the measured refractive index as a function of time, n_{IL} is the measured refractive index of the dry IL (1.48, 1.42, and 1.37 for vacuum-dried [EMIM][$EtSO_4$], [EMIM][TFSI], and [EMIM][FAP]); n_{water} = 1.33 is the refractive index of water; and ϕ is the volume fraction of water. The refractive index of the ILs was also determined in equilibrium with the selected humid environment, but only the values for [EMIM][$EtSO_4$] were observed to vary (see Table 1).

When the environmental humidity was increased from 0% to 15% RH, both the film thickness and the refractive index of the selected ILs did not noticeably change during a period of 8 h. Note that the water-to-IL mole ratio increases to 0.23 ± 0.03 and 0.03 ± 0.02 in unconfined [EMIM][$EtSO_4$] and [EMIM][TFSI], which corresponds to a volume fraction of water (ϕ) of ~2.16% and ~0.24%, respectively. The negligible variation of D and n suggests that the water uptake by the nanoconfined IL films is too small or too slow to be sensed.

3.1.1. [EMIM][$EtSO_4$] Confined between Mica Surfaces. The surfaces were then separated to D > 1 μm, equilibrated longer at 15% RH, and approached again to D ~ 3.7 ± 0.5 nm before the humidity was increased to 35% RH. After ~50 min, the water uptake by [EMIM][$EtSO_4$] led to a decrease of both the film thickness and the refractive index (Figure 1a). The reproducible decrease in film thickness occurred in two steps (Δ_1 ~ 0.77 nm and Δ_2 ~ 0.48 nm). The first squeeze-out (Δ_1) was accompanied by a concurrent drop in refractive index from 1.42 ± 0.01 to 1.38 ± 0.01, which implies that ϕ increased from ~40% to ~67%, according to eq 9. These concurrent events imply that an IL-rich layer was squeezed out. The second squeeze-out event (Δ_2) did not involve an abrupt change in n, which means that both ions and water left the confined region so that ϕ remained approximately constant. Later, the refractive index slowly decreased to ~1.35 ± 0.01, which indicates that the volume fraction of water increased to ~86%. Here, it is possible that water slowly diffused into the

DOI: 10.1021/acsami.9b10923
ACS Appl. Mater. Interfaces 2019, 11, 33465–33477

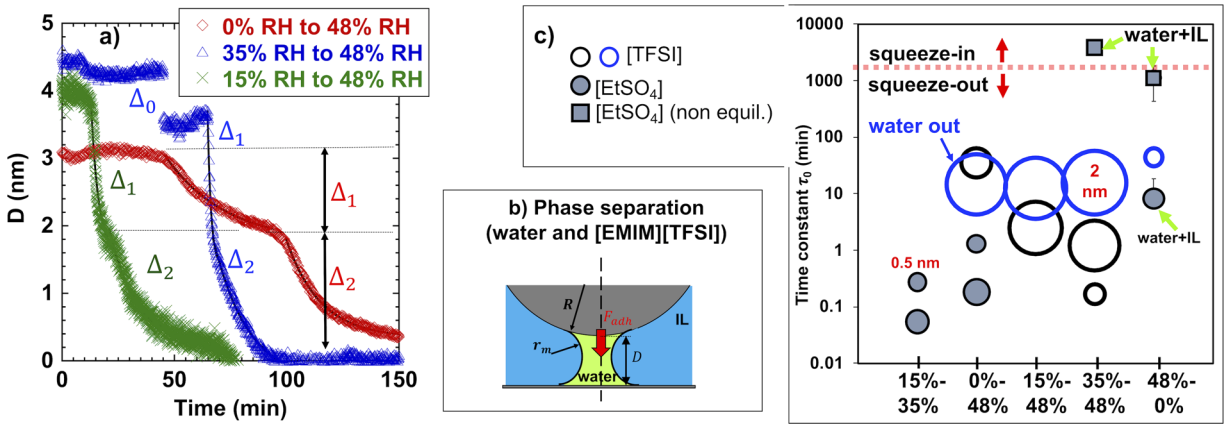

Figure 2. (a) Time-dependent drainage of [EMIM][TFSI] upon an increase in the relative humidity to 48 ± 3%; the ILs were initially equilibrated at three different conditions (red diamonds = 0% RH, green crosses = 15% RH, and blue triangles = 35% RH). The black lines illustrate fits of $D(t) \approx a + b \times \exp(-t/\tau_0)$ to the experimental data. (b) Schematics showing the phase separation between water and [EMIM][TFSI] in the confined geometry. (c) Bubble diagram with the time constants τ_0 for [EMIM][TFSI] (empty bubbles) and [EMIM][$EtSO_4$] (filled bubbles/squares). The experimental conditions are given in the *X*-axis as the initial and final relative humidities in the diffusion experiments. The size of two bubbles (Δ = 0.5 and 2 nm) are given for guidance. The filled squares indicate that equilibrium was not achieved during the duration of the experiment with [EMIM][$EtSO_4$]. Some error bars are smaller than the symbol size and not shown for clarity.

confined film, as inferred from the small and slow increase in *D* over several hours (see arrow). Note that the refractive index is smaller than that of the unconfined IL at 35% RH (~1.466, Table 1), which is attributed to the higher water content in films of less than 4 nm in thickness.

The surfaces were then separated, equilibrated at ~35% RH, and approached again to ~3.7 nm. When the relative humidity was further increased to ~48% RH (Figure 1b), a slow expansion of the film from 3.49 to 4.06 nm was recorded (Δ_1 ~ 0.57 nm). The initial decrease in the refractive index from ~1.38 ± 0.01 to ~1.36 ± 0.01 supports that water spontaneously entered into the film upon the increase in humidity, leading to an increase in the volume fraction of water from 67% to 77%. The film thickness changed in a slow fashion over 10 h without achieving equilibrium, while the refractive index remained constant, which suggests that IL ions and water entered the confined region so that ϕ did not vary with time. The uptake of [EMIM][$EtSO_4$] and water together is consistent with the strong hydrogen bonding between water and this IL.[31]

The surfaces were then separated to $D > 1$ μm to equilibrate the system at ~48% RH for a longer time, the IL was confined again, and the SFA cell was continuously purged with a gentle stream of dry nitrogen (Figure 1c). Here, a two-step squeeze-out of the IL was reproducibly observed: first, an immediate decrease in film thickness (Δ_1 ~ 0.5 nm) followed by a slower decrease in film thickness that did not achieve equilibrium after 8 h (Δ_2 ~ 0.5 nm). While following different kinetics, the refractive index increased from 1.36 ± 0.01 to 1.39 ± 0.02. The initial drop of the film thickness (Δ_1) occurred while the refractive index remained approximately constant, which suggests that both water and ions spontaneously left the confined space so that their volume fractions in the confined film remained unchanged. The following increase in refractive index by ~0.03 indicates that the volume fraction of [EMIM][$EtSO_4$] increased by roughly 20% while *D* remained constant, which supports the exchange of water by IL. The subsequent slow decrease in *D* while *n* remained constant supports the spontaneous squeeze-out of ions and water.

3.1.2. [EMIM][TFSI] Confined between Mica Surfaces. The confined [EMIM][TFSI] did not respond to an increase of relative humidity to 35%, which indicates that the uptake of water, if it happened, was too small to be detected as a change of *D* or *n*. Based on the dynamic force measurements discussed later, it is likely that water does diffuse into the confined liquid film, but the change is too slow or too small to be detected. The small water uptake by this IL compared to [EMIM]-[$EtSO_4$] (Table 1) justifies that a higher ambient humidity may be required for a change in film thickness to be measurable in this type of experiment. When the relative humidity was increased to ≳45%, a spontaneous drainage of the IL was reproducibly measured so that the two surfaces came into adhesive contact (see Figure 1e; note the different scale of the *Y*-axis compared to Figure 1a–c). During the squeeze-out process, the refractive index first decreased from ~1.42 ± 0.01 (close to the value of the dry IL) to ~1.38 ± 0.02 (Δ_0 ~ 0.78 nm), indicating that ions left, and water diffused into the confined space, achieving a volume fraction of water of ~44%. During the second squeeze-out event (Δ_1 ~ 0.96 nm), the refractive index achieved the value corresponding to water. Then, the refractive index became unstable and abruptly decreased to zero. This happens because the numerical method used to evaluate the interference cannot determine the refractive index close to mica–mica contact, as described in the Experimental Methods section. After conclusion of the liquid drainage (D ~ 0 nm), the pull-off force increased to ~152 ± 42 mN/m, which is ~25 times larger than for [EMIM][$EtSO_4$] (5.3 ± 1.2 mN/m) at 48% RH. A van der Waals force cannot account for such a high pull-off force, since this would require a Hamaker constant about 1 and 2 orders of magnitude larger than the values expected for [EMIM][TFSI] (8.42×10^{-21} J) and water (2×10^{-20} J), respectively.

The squeeze-out of [EMIM][TFSI] also happened when the liquid was initially equilibrated at 0% and 15% RH, confined to ~3–4 nm and then exposed to 48 ± 3% RH (Figure 2a). This behavior is reminiscent of the phase separation that occurs when nonpolar solvents like octamethylcyclotetrasiloxane (OMCTS) are confined between mica surfaces and exposed

DOI: 10.1021/acsami.9b10923
ACS Appl. Mater. Interfaces 2019, 11, 33465–33477

to humid air.[32] The higher affinity of water to mica and its immiscibility with the solvent have been recognized to induce this phase separation upon nanoconfinement. This phenomenon is thermodynamically analogous to capillary condensation, which happens when a gas confined in a nanopore condenses to a liquid at a relative pressure below that corresponding to the liquid−vapor coexistence in the bulk. The Kelvin equation gives the relation between the interfacial tension between immiscible liquids (γ_{IL-w}) and the radius of curvature of the meniscus (r_m) as $RT/V_w \ln a_w = \gamma_{IL-w}/r_m$, where V_w is the molecular volume of the solute (water here) and a_w the activity of the solute in the organic solvent (here the IL); a_w equals the relative humidity in the gas phase.

If a bridge of water forms between the two surfaces, the water−IL interface will have a negative curvature (Figure 2b), and the resulting Laplace pressure difference across the meniscus will pull the surfaces together yielding a pull-off force $F_{adh} = 4\pi R\gamma_{IL-w} \cos\theta$, where θ is the contact angle for water on mica.[33] The contact angle was not measured in our experiments, but we take $\theta \leq 10°$ based on previous studies.[33] For the measured pull-off force of 152 mN/m, this assumption yields $\gamma_{IL-w} = 12.2 \pm 0.1$ mJ/m^2, in reasonable agreement with the reported value for this IL (9.85 mJ/m^2).[34] On the other hand, the geometry of SFA experiments establishes that phase separation should spontaneously occur when $D \sim d + 2r_m \cos\theta$, d being the thickness of the adsorbed water molecules on mica, if present.[35] Using the Kelvin equation to determine r_m at $a_w = 0.48$ (48%RH) and assuming the adsorption of a monolayer of water on each mica surface ($d \sim 0.54$ nm), this expression yields that phase separation between [EMIM][TFSI] and water should happen at $D \sim 0.79$ nm. This calculation often underestimates the actual surface separation,[35,36] mainly because the Kelvin equation breaks down at such small separations. Nevertheless, these simple estimations support that a surface-induced phase separation can happen when [EMIM][TFSI] is confined in ∼3−4 nm hydrophilic pores in equilibrium with humid air above ∼45% RH.

Based on this, we propose that water molecules diffuse into the thin films of [EMIM][TFSI] due to their strong affinity to mica, either through the bulk IL or along the mica surfaces. The increased water content in the thin film at ∼45% RH and its immiscibility with [EMIM][TFSI] are responsible for phase separation and, thereby, for the squeeze-out of the IL during the first drainage steps (Δ_0 and Δ_1) (Figures 1e and 2a). This leads to the growth of a capillary meniscus and, thereby, to the action of an attractive capillary force that deflects the spring and brings the surfaces closer to each other, thereby justifying the squeeze-out of water (Δ_2). Note that water is miscible with [EMIM][EtSO$_4$] at any mole ratio,[29] which prevents this phenomenon from happening in this case. However, this phenomenon should be universal for other ILs that are not fully miscible with water, when confined between hydrophilic surfaces at sufficiently high environmental humidity. Since [EMIM][TFSI] and water are miscible at 50% RH in the unconfined state, this implies that the water content in the confined geometry must exceed the content in the liquid reservoir, which is consistent with the measured refractive index. A phase separation between this IL and water has also been proposed based on static force measurements.[37]

In selected experiments, the surfaces were slowly separated only to ∼4 nm to maintain this meniscus, and then dried at 0% RH (Figure 1f). Here, the refractive index remained constant at ∼1.33 ± 0.03 and the film thickness decreased by $\Delta_1 \sim 0.9$ nm, which indicates that water abandoned the confined film, but no significant number of ions entered the confined space. This differs from the results for [EMIM][EtSO$_4$], where an exchange of water by ions was inferred from the experimental results (see, e.g., Figure 1c). The different behavior is attributed to the immiscibility between [EMIM][TFSI] and water, as such an exchange would require that the IL diffuses through a capillary meniscus into the water film. To separate the surfaces under these conditions, a pull-off force of at least 1229 ± 30 mN/m had to be applied. The stronger pull-off force supports that drying led to the retraction of the IL−water meniscus, and thereby to a stronger capillary force that held the two mica surfaces together. These results also suggest that water can remain trapped in a hydrophilic nanopore when the system is exposed to a dry environment.

3.1.3. Time Constants. Our attempts to determine a diffusion coefficient from these experiments failed due to the complexity of this process; note that it involves not only the diffusion of water into the confined region but also a change of the mechanical equilibrium, which leads to the motion of the surface and the squeeze-out of the liquid. Therefore, to compare the rates of squeeze-in and -out across the experiments, an exponentially decaying function $D(t) \sim a + b \times \exp(-t/\tau_0)$ was fit to the experimental results (e.g., see lines in Figure 2a). According to this expression, larger time constants (τ_0) represent a slower event. Figure 2c shows the time constants (τ_0) at the conditions given in the X-axis: from 15% to 35% RH, from 0% to 48% RH, from 15% to 48% RH, from 35% to 48% RH, and from 48% to 0% RH; note that the condition 15−48% was only investigated for [EMIM][TFSI]. The size of the symbols has been chosen to be proportional to the change in film thickness (Δ), and it clearly shows that higher changes in film thickness occur in the case of the hydrophobic IL when exposed to environmental humidity.

For the majority of conditions, a change of humidity caused a squeeze-out of the confined ILs. The fact that more than one symbol is given for each condition reflects the quantized nature of the process, since the film thickness did not decrease gradually but as a sequence of steps (Δ_1, Δ_2, etc.). For instance, this happened to [EMIM][EtSO$_4$] when the RH was increased from 15% to 35% RH. Here, τ_0 increased from 0.05 (for Δ_1) to 0.27 min (for Δ_2), which implies that the squeeze-out of the IL became slower as both the film thickness D and the gradients between the water activity in the reservoir and in the confined film decreased over time. This happened at all conditions. The humidity increase from 0% to ∼48% RH reveals another important finding. Although [EMIM][EtSO$_4$] and its mixtures with water have a bulk viscosity higher than or similar to that of [EMIM][TFSI] (116−33 vs 32 mPa.s, Table 1), the time constants for the squeeze-out of [EMIM][EtSO$_4$] are up to 2 orders of magnitude smaller (τ_0 ∼0.1 to ∼1 min vs 35 min). This suggests that the *bulk* viscosity of the IL is not the main factor determining the drainage of the liquids. Upon drying, the time constant for the squeeze-out of [EMIM][EtSO$_4$] along with that of water achieved very high values (τ_0 ∼8.17 to 1123 min), reflecting that the drainage became gradually hindered as both the film thickness and content of water in the film decreased.

The diffusion experiments with [EMIM][TFSI] only allowed investigation of the kinetics of phase separation. The time constants during the initial stage of phase separation between water and [EMIM][TFSI] at 48% RH (Δ_0 and Δ_1) depend significantly on the initial water content in the IL prior

DOI: 10.1021/acsami.9b10923
ACS Appl. Mater. Interfaces 2019, 11, 33465−33477

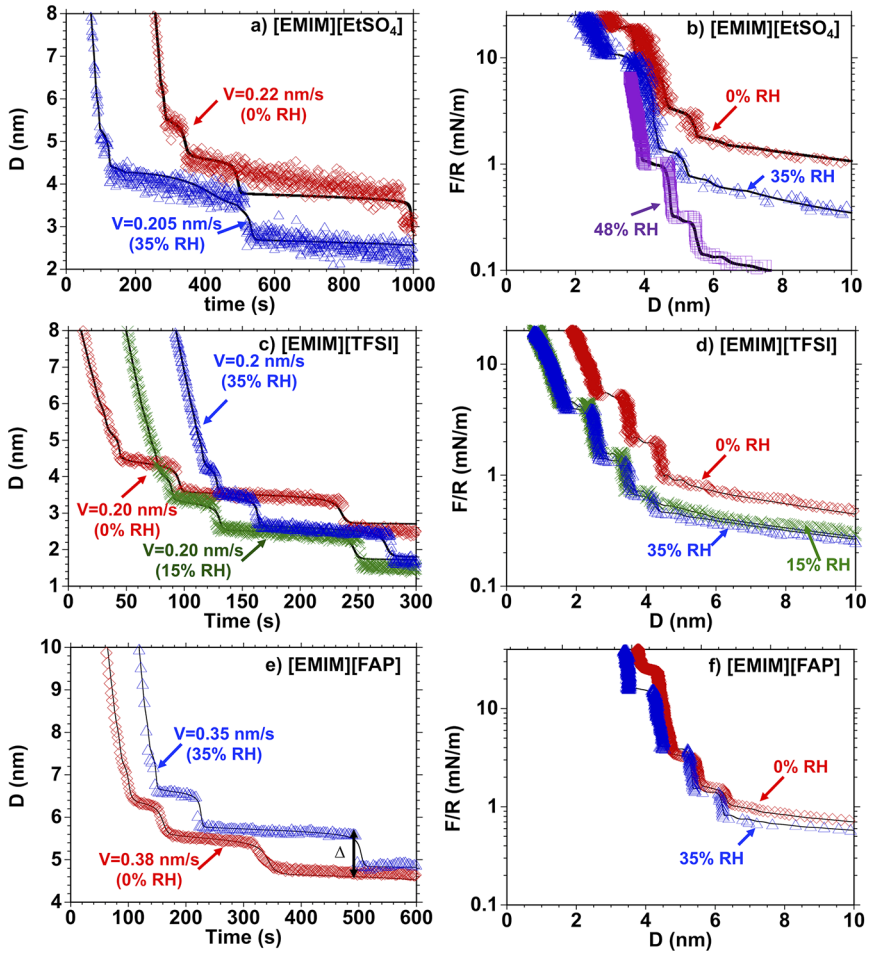

Figure 3. Representative measurements of film thickness with time ($D(t)$, left) and spring force as a function of surface separation ($F(D)$, right) for (a,b) [EMIM][$EtSO_4$], (c,d) [EMIM][TFSI], and (e,f) [EMIM][FAP], at selected RHs (red diamonds = 0% RH, green crosses = 15% RH, blue triangles = 38% RH, and purple squares = 50% RH). The approach velocity of the piezo (V) is given for the selected experiments. The black lines show the fits to the experimental data represented by the markers.

to confinement (equilibrated at 0%, 15%, or 35% RH). Importantly, higher initial water concentrations are associated with smaller time constants (~35 min (0%RH), ~2.5 min (15%RH), and ~0.16−1.2 min (35%RH), i.e., with a faster squeeze-out of [EMIM][TFSI]. In contrast, the squeeze-out of water due to the action of the capillary force follows similar kinetics under all conditions (τ_0~12 ± 2 min for Δ_2, see blue bubbles), which supports that the three systems undergo the same type of transition, as discussed earlier.

3.2. Dynamic Force Measurements. Dynamic force measurements were conducted to quantify the influence of the environmental humidity on the interfacial structure, electrostatics, and dynamics of hydrophilic and hydrophobic ILs confined between mica surfaces. Here, the ILs were first equilibrated with a humid environment in the unconfined state ($D > 1$ μm), and then, one of the surfaces was approached at a constant velocity (V) so that hydrodynamic effects became relevant. Figure 3 shows representative measurements of $D(t)$ and $F(D)$ from dynamic force measurements for [EMIM]-[$EtSO_4$], [EMIM][TFSI], and [EMIM][FAP], the latter being more hydrophobic than [EMIM][TFSI] (Table 1).

3.2.1. Interfacial Structure. The steps in Figure 3 result from the pressure-induced outflow of layers of ions and water, and hence, they reflect the quantized structure of the confined films, in agreement with previous works.[14,24,38,39] This step size is not strictly equal to the true thickness of the molecular layer, but to the change in the film thickness when a layer is squeezed out of the thin film ($\Delta = D_I - D_F$), D_I and D_F being the film thickness at which the transition starts and ends, respectively. For conciseness, we will refer to Δ as the layer thickness. The average size of the steps as a function of D_I is shown in Figure 4a−c for the three ILs.

The different layer thicknesses of the selected ILs reflects the effect of the anion on the interfacial structure, and it is Δ ~ 0.81 ± 0.05, 0.72 ± 0.03, and 0.71 ± 0.04 nm for dry [EMIM][$EtSO_4$], [EMIM][TFSI], and [EMIM][FAP], respectively, in good agreement with previous works.[11,14] This size is consistent with a monolayer structure composed of both cations and anions alike (abbreviated as "monolayer"). For instance, the molecular volume (Ω) of [EMIM][TFSI] and [EMIM][FAP] yields an ion pair diameter of $\Omega^{1/3}$ ~0.75 nm and ~0.81 nm, respectively. The decrease of Δ with a decrease in film thickness is evident in the case of dry [EMIM][$EtSO_4$] and [EMIM][FAP]. While we cannot exclude that this results from the compressibility of these ILs, it is also possible that the measurement of the layer thickness in dynamic force measurements becomes less precise as the film thickness decreases, especially for these two ILs with highest viscosity.[11]

Upon exposure of the ILs to a humid environment, the interfacial layered structure is maintained, but an expansion of

DOI: 10.1021/acsami.9b10923
ACS Appl. Mater. Interfaces 2019, 11, 33465−33477

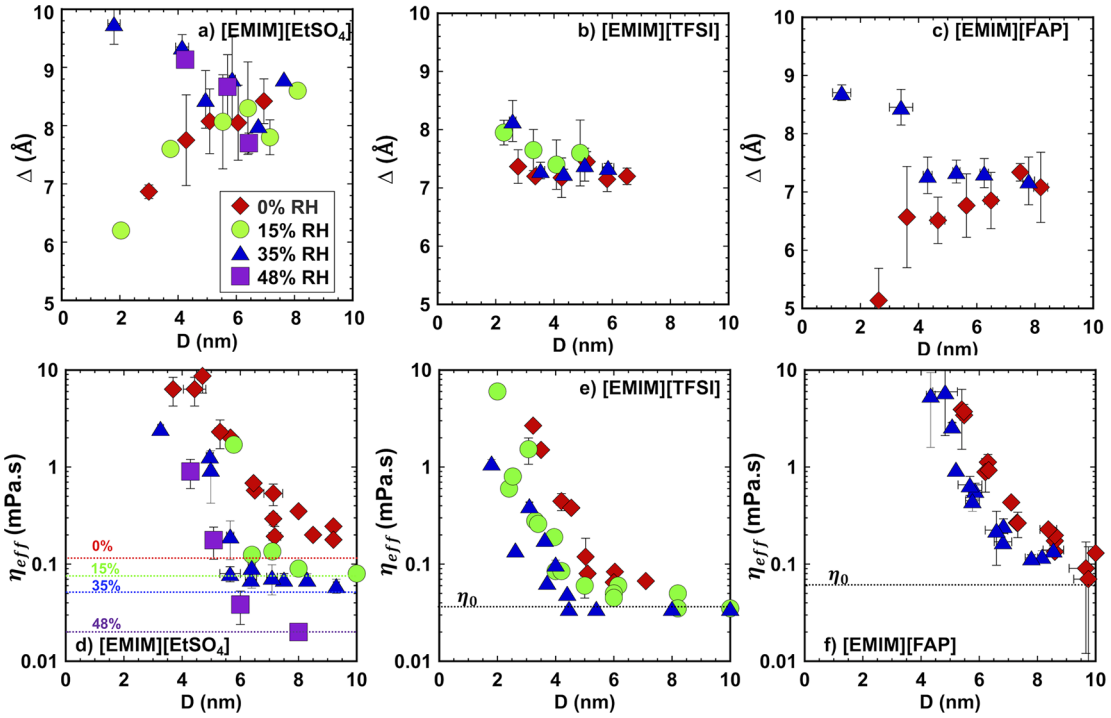

Figure 4. (a–c) Step size (Δ) vs film thickness (D) and (d–f) effective viscosity (η_{eff}) vs film thickness (D) for (a,d) [EMIM][$EtSO_4$], (b,e) [EMIM][TFSI], and (c,f) [EMIM][FAP]. The dashed lines represent the bulk viscosity (η_0). The different colors in (d) represent the bulk viscosity at the corresponding ambient humidity: red (0% RH), green (15% RH), blue (35% RH), and purple (48% RH); see Table 1. Note that the step size is given here in angstroms.

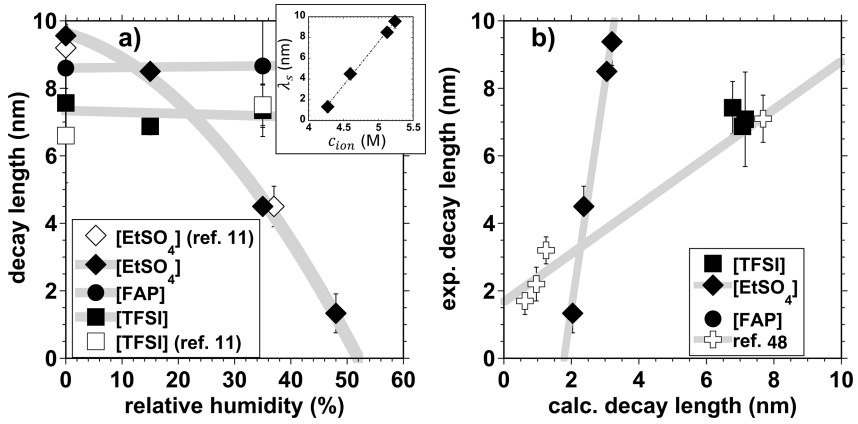

Figure 5. (a) Influence of the relative humidity on the measured decay length of the electrostatic interactions (λ_s) for the selected ILs. The inset shows λ_s as a function of the ion pair concentration (c_{ion}) in [EMIM][$EtSO_4$] equilibrated at different RHs. (b) Relation between the experimentally determined decay length and the calculated decay length according to $\lambda_{calc} \sim a^3 c_{ion} l_B$; see ref 47. Calculated values for the ion diameter according to $a \sim 1/2 \times V_{mol}^{1/3}$, V_{mol} being the molecular volume of the ion pair: 3.77, 3.41, 4.07, and 2.94 Å for [EMIM][TFSI], [EMIM][$EtSO_4$], [EMIM][FAP], and NaCl, respectively. The crosses in (b) are data for NaCl and [EMIM][TFSI] from ref 48 to illustrate the agreement with the scaling relationship.

the step size with a decrease in film thickness is observed for the three ILs in the range of investigated humidities. This expansion is sensitive to the specific anion in the IL. In the case of [EMIM][$EtSO_4$], the increase of the humidity to 15% RH did not lead to any clear change in step size (Figure 4a), although the water content in the bulk (unconfined) IL is quite remarkable (4.3 ion pairs per water molecule). This indicates that this IL can accommodate a large amount of water with no measurable change of interfacial structure; more details about the interfacial structure are given in the Discussion section. At 35% and 50% RH, the step size increased from 0.84 ± 0.04 nm at D ~8 nm to ~0.98 ± 0.03 nm at D ~ 2 nm. Despite the prominent hydrophobicity of [EMIM][FAP], a pronounced expansion of the step size to ~0.87 ± 0.02 nm at D < 3 nm was measured when the humidity was increased to 35%. In [EMIM][TFSI], a smaller increase from 0.72 ± 0.03 nm to ~0.82 ± 0.03 nm at D ~ 2.5 nm was observed at both 15% and 35% RH, which supports the presence of interfacial water. This also suggests that the water uptake was not detected in diffusion experiments because the rate was too small to be distinguished from the drift of the instrument. Note that [EMIM][TFSI] and [EMIM][FAP] were not exposed to higher relative humidity to avoid phase separation during dynamic force measurements.

DOI: 10.1021/acsami.9b10923
ACS Appl. Mater. Interfaces 2019, 11, 33465–33477

The results in Figure 4a–c suggest that the water molecules are accommodated in the confined films of the three ILs. The results agree well with previous force measurements that showed the influence of water on the interfacial structure of ILs on mica.[37,40−43] Previous MD simulations have also shown that water accumulates near a hydrophilic surface like mica and leads to a reorientation of the ions due to the induced change of intermolecular interactions.[16,44] Our measurements cannot determine how the intercalated water molecules modify the ion arrangement, though, but it is interesting that, despite the different water uptake by the three ILs in unconfined state, the observed expansion of the layer thickness is similar, especially in the case of [EMIM][FAP] and [EMIM][$EtSO_4$]. This suggests that the water content in the thin films confined between hydrophilic (mica) surfaces is strongly affected by the hydrophilic nature of the mica surface.

3.2.2. Screening Length. To determine the decay length of the electrostatic long-range force, eq 8 was integrated and $D(t)$ and $F(D)$ fit to the experimental results for separations between ∼10 and ∼100 nm, with D_s, η, B, and λ_s being fitting parameters (Table S2). In our previous dynamic force measurements on six different vacuum-dried imidazolium ILs, a good fit to the experimental results was achieved assuming that the viscosity is equal to the bulk viscosity $\eta = \eta_0$ with a stick length $2D_s \sim 3.6 \pm 0.4$, 3.9 ± 0.4, and 3.2 ± 0.5 nm for vacuum-dried [EMIM][$EtSO_4$], [EMIM][TFSI], and [EMIM][FAP], respectively. This implies that ∼2−3 monolayers (each composed of ion pairs) remain immobilized on each mica surface during the drainage of the dry ILs. Here, we have found that the stick length decreased to approximately zero ($2D_s \sim 0$) upon equilibration of the ILs in the humid environment, while $\eta = \eta_0$. This suggests that the presence of water facilitates the motion of the ions close to the solid−liquid interface.

A long-range electrostatic force (F_{el}) was detected under all conditions. This indicates that the surface is charged—in the case of mica, negatively charged in contact with an IL—,[22] the surface-adsorbed ions cannot completely screen the surface charge, and an electrical double layer builds up to screen the negative charge. The decay length of the electrostatic force (λ_s) is depicted in Figure 5a as a function of the relative humidity. For the dry ILs, the screening length ranges between ∼6.5 and 10 nm. To explain such long-range screening, it has been proposed that ILs consist of an effectively neutral, coordinated cation−anion network in dynamic equilibrium with a small fraction of dissociated ions that effectively screen the charge (<0.007%).[22] This amount is much smaller than that inferred from ion diffusivity and electrical conductivity measurements (∼60%)[45] and from recent simulations (∼15%),[46] and hence, this work cannot yet resolve this controversial subject.

A prominent drop in λ_s with relative humidity was obtained for [EMIM][$EtSO_4$], which results in a linear relation between the ion pair concentration (c_{ion}) and λ_s (see inset). In contrast, λ_s does not appreciably depend on the humidity in the case of [EMIM][TFSI] and [EMIM][FAP] ($\lambda_s \sim 6.9 \pm 0.8$ nm and $\lambda_s \sim 8.6 \pm 0.9$ nm, respectively). This is reasonable considering that the screening length of electrostatic interactions is an intrinsic property of the unconfined ILs,[47] and the water uptake by these ILs is small.

3.2.3. Effective Viscosity. At separations smaller than 10 nm, van de Waals and solvation forces cannot be neglected, so that the force balance is given by eq 7. The assumption that the viscosity of the nanoconfined IL remains equal to its bulk viscosity does not provide a good fit to the experimental results in this case. Since an independent determination of D_s and η is not possible, we arbitrarily introduce an effective viscosity η_{eff} to describe the viscous drag so that[11]

$$F_{visc} = -\frac{6\pi R^2 \eta}{D - 2D_s}\frac{dD}{dt} = -\frac{6\pi R^2 \eta_{eff}}{D}\frac{dD}{dt} \quad (10)$$

This expression presumes that due to the proximity of the two surfaces, all the ions are equally slowed down, i.e., the mobility of the liquid molecules is uniform across the confined film. Fitting the trajectory of the surface $D(t)$ and the spring force $F(D)$ to the experimental data requires refining the fitting parameters η_{eff}, C, λ_1, and λ_2 iteratively, while A, V, B, and λ_s are known. C, λ_1, and λ_2 must remain constant in a single trajectory, while η_{eff} is allowed to vary with the film thickness. Here, it is assumed that the effective viscosity does not change continuously during the drainage but in a discrete or quantized fashion at the end of each step. Therefore, the effective viscosity is adjusted after each layer is squeezed-out until a good fit to the experimental data is achieved. Due to the error induced by the deformation of the epoxy glue, and neglected in the proposed model, only data corresponding to F/R smaller than 20 mN/m were fit to ensure that the sphere-plane geometry still applies.[11] The lines in Figure 3 demonstrate the good fit of the calculated trajectory and force to the experimental results with the effective viscosity that is shown in Figure 4d–f. We emphasize that some layers were occasionally not clearly resolved (see e.g. Figure 3a, time ∼600 s), and especially at high loads, which is believed to be caused by the continuous motion of the surfaces in dynamic force measurements.[49] The values of A, B, C, λ_1 and λ_2 are given in Table S2.

Figure 4d–f shows that the effective viscosity of the three *dry* ILs increases by about 2 orders of magnitude from the bulk value upon confinement to a film thickness of $D \sim 3$ nm. This is in qualitative agreement with the increase in viscosity of the confined films (of similar thickness) of other imidazolium ILs determined by resonance shear measurements.[50] Note that each symbol usually represents the average of 3 measurements and that the standard deviation is often smaller than the symbol size, and therefore not always visible. The clusters are a consequence of the model for the effective viscosity, which assumes that the viscosity increases after each step. Note that the step size corresponding to the effective viscosity at $D \sim 8$−10 nm is not shown in Figure 4a–c because it cannot be determined with precision. For a given film thickness, the effective viscosity of [EMIM][TFSI] is about 1 order of magnitude smaller than that of [EMIM][FAP] and [EMIM]-[$EtSO_4$] (see Figure S2 in the Supporting Information for better comparison). This coincides with the smaller range and magnitude of its solvation force, which are typically associated with a weaker interfacial structure. This difference is more prominent than between the bulk viscosities of the dry ILs.

Figure 4d–f also shows the influence of water on the effective viscosity of the confined ILs. The effective viscosity is observed to decrease by up to 1 order of magnitude upon an increase in RH; see, e.g., [EMIM][$EtSO_4$] and [EMIM]-[TFSI]. The decrease in effective viscosity appears less remarkable for [EMIM][FAP], but it is still statistically significant. We thus conclude that the intercalated water molecules in the confined ILs facilitate the drainage of the three selected ILs sandwiched between mica surfaces.

DOI: 10.1021/acsami.9b10923
ACS Appl. Mater. Interfaces 2019, 11, 33465−33477

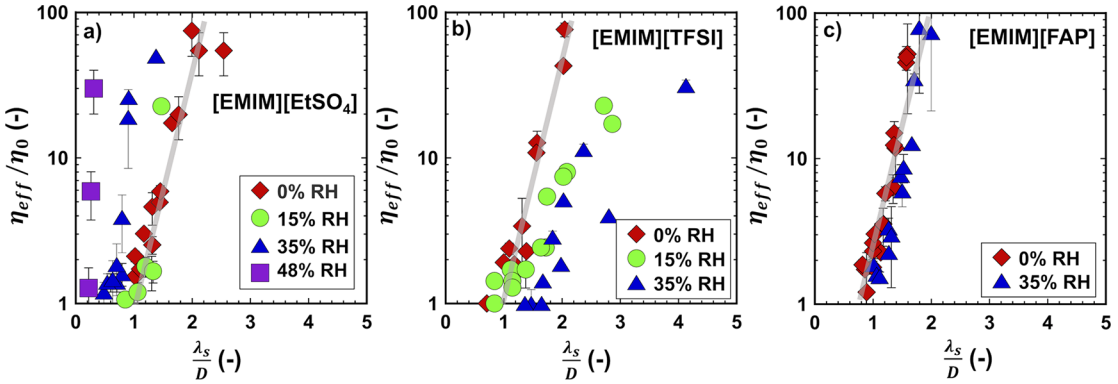

Figure 6. Ratio between effective viscosity and bulk viscosity (η_{eff}/η_0) vs ratio of screening length and film thickness at which each step takes place (λ_s/D), for (a) [EMIM][$EtSO_4$], (b) [EMIM][TFSI], and (c) [EMIM][FAP]. The red diamonds represent data measured in the dry environment, green circles for 15% RH, blue triangles for 35% RH, and purple rectangles for 50% RH. The gray line represents the exponential relation reported in ref 11 for the dry ILs.

4. DISCUSSION

Our diffusion experiments simulate the wetting of nanopores (with hydrophilic and charged surfaces) filled with ILs upon exposure to ambient humidity. Given sufficient time, it is expected that water will enter the hydrophilic nanopores and will lead to a partial exchange of the ions by water. In the case of ILs that are not fully miscible with water (here, [EMIM][TFSI]), surface-induced phase separation will occur in the nanopore at sufficiently high environmental humidity (while it is excluded in the unconfined state) and the IL will be completely replaced by water in the nanopore. The relative humidity for phase separation in the nanopore is dictated by the specific interfacial energy of the immiscible liquids, the contact angle of water on the pore surface, and the pore size, as given by the Kelvin equation in analogy to capillary condensation. In contrast, if the IL is fully miscible with water, it remains in the pore, but the volume fraction of water may exceed the bulk concentration, as inferred from the measured refractive index of the confined ionic liquids.

In equilibrium with humid air (and excluding phase separation), water molecules are intercalated into the layered structure of hydrophilic and hydrophobic ILs in hydrophilic nanopores, and more so close to the liquid−solid interface. Interestingly, the interfacial structure of [EMIM][$EtSO_4$] is in notable contrast to those reported for mixtures of [C_4C_1Pyrr]-[TFSI] with a solvent, propylene carbonate, also miscible at any ratio with the IL.[51] Here, an abrupt change of the periodicity of the oscillatory force (step size) was measured with the change in IL concentration. Below a threshold concentration, the periodicity was determined by the size of the solvent molecule (0.55 nm), whereas above the threshold, it was given by the diameter of the cation−anion pair (0.8 nm). It is interesting that, although propylene carbonate and [C_4C_1Pyrr][TFSI] are miscible at all ratios, the confined films were not a mixture of both, but instead, they were composed of one or the other depending on the concentration. Our results for [EMIM][$EtSO_4$] are in better agreement with the pioneering work by Horn et al.[24] Here, it was shown that, as water was added progressively to ethylammonium nitrate, the range of the oscillatory force and the number of oscillations in the force decrease markedly, but the periodicity remained approximately constant (~0.5 nm); a similar behavior was also reported for OMCTS (periodicity ~0.8 nm) and water.[36] These works suggested that, if two molecular species of different size are present in the confined space, there are more possible ways to fill a given space, i.e., fewer packing restrictions. This leads to fewer layers and weaker solvation forces. A decrease of the magnitude of the oscillatory force is, in fact, seen for the three investigated ILs when water is present in the system (Figure 3b,d,f), and hence, the change of the interfacial structure of the three ILs induced by the exposure to a humid environment seems consistent with this steric argument. The hydrogen bond between the cation and the anion in [EMIM][$EtSO_4$] with water might be responsible for the ability to hold large amounts of water through a small expansion of the interfacial layers. In fact, a similar behavior was reported for 1-hexyl-3-methyl imidazolium [$EtSO_4$] by our group before.[43]

The main difference from previous work on nonpolar solvents arises from the ionic nature of ILs. Dynamic force measurements yield screening lengths ranging between ~10 and ~1.5 nm (Figure 5a). Figure 5b shows the measured screening length (λ_s) vs the calculated screening length (λ_{calc}) according to ref 47, i.e., $\lambda_{calc} \sim a^3 c_{ion} l_B$, l_B being the Bjerrum length, c_{ion} the ion pair concentration, and a the mean ion diameter. This expression is based on the ionic semiconductor concept, which implies that the ions are associated and behave like a dielectric medium, whereas "defects" (solvent, dissociated ions, etc.) are the effective charge carrier that build up the electrical double layer on a charged surface. The crosses represent data points for NaCl solutions from ref 48 to illustrate the trend given by this scaling law (gray line in Figure 5b); our data for [C_2C_1Im][TFSI] agree well with λ_{calc}.

Although the deviation of [C_2C_1Im][$EtSO_4$] from this scaling relationship was already reported in our previous work,[11] the new data in the inset in Figure 5a clearly prove that the linear relation between c_{ion} and λ_s prevails upon wetting. For these calculations, the relative dielectric constant of this IL in the dry state was taken as 27.9 (−) from ref 52, the effective medium theory[26] was used to calculate the influence of the volume fraction of water (e.g., it increases to 36 (−) for 18.7 vol % of water), and a was assumed to remain constant and equal to 0.341 nm. In the dry state, the scaling relationship underestimates the screening length, and the abrupt decrease in λ_s with an increase in water content is more significant than predicted based on the volume fraction of water. As inferred from IR spectroscopy,[11] the anion−cation hydrogen bond network is significant in this IL, while water hydrogen bonds

DOI: 10.1021/acsami.9b10923
ACS Appl. Mater. Interfaces 2019, 11, 33465−33477

with anion and cation at mole ratios of water to IL >1.5 and weakens the anion−cation hydrogen bond network. It is, therefore, possible that the prominent hydrogen bonding in this IL enhances ion association in the dry state and that the distortion of the hydrogen bond network by water promotes ion dissociation, and thereby the decrease in the screening length. Although still speculative, this suggests that the scaling relationship for λ_{calc} is not robust to varying chemical functionalities.

The effective viscosity in Figure 4d−f characterizes the mobility of the confined ILs in hydrophilic and charged nanopores as a function of ambient humidity. The effective viscosity increases by up to 2 orders of magnitude with a decrease in the film thickness from ∼10 to ∼3 nm for the three *dry* ILs. A similar increase in viscosity has been observed for other nonpolar solvents that arrange in layers under nanoconfinement,[10] and hence, this is not a unique property of the confined ILs. Prolonged molecular relaxation times are generally associated with the restricted motion of the molecules within and across layers and to the interactions with the surface. However, ILs flow along a charged surface, and hence, one could also expect a coupling between electric and viscous effects. Recently, a quasi-exponential relation between η_{eff}/η_0 and λ_s/D was reported for six different *dry* ILs,[11] which is represented by the gray line in Figure 6. Based on Levine's precedent work for dilute electrolytes,[53] it was hypothesized that the increase in viscosity could be partially originated by the so-called "electroviscous retardation". Our additional data in the presence of water, however, deviate from this exponential relation, as demonstrated in Figure 6a−c, which motivates us to revise this hypothesis and look for alternative explanations.

In general, the flow rate of confined fluid films depends on the friction coefficient among the liquid molecules and at the liquid−solid interface.[54] Such molecular friction is presumably higher in ILs compared to nonpolar solvents due to the action of Coulombic forces. In this context, a recent experimental and MD study has shown that the ion mobility of highly concentrated NaCl solutions is reduced by a factor of 3 from the corresponding bulk value in pores with a diameter smaller than 5 nm; dilute solutions, in contrast, flow faster through narrow spaces.[55] It appears that ion pairing in concentrated electrolytes as well as collisions between ions of opposite charges contribute to the reduced mobility. In situ NMR corroborate that Coulombic interactions in ILs are a key contributor to the reduced diffusivity of the liquid in nanopores due to the enhanced association of oppositely charged ions.[8] Furthermore, it has been shown based on thermodynamic arguments that ion association in ILs is favored under nanoconfinement due to the free energy penalty caused by the suppressed lattice expansion upon ion-pair dissociation.[56] All this suggests that the increase in viscosity upon nanoconfinement might reflect the increase in anion−cation association, deviating from the bulk behavior. It is, therefore, reasonable to expect that promoting a greater degree of ion dissociation under nanoconfinement could afford reduced viscosity and higher conductivity of the ILs.

The change of the interfacial structure (Figure 4a−c) demonstrates that water molecules are intercalated into the anion−cation network of both hydrophobic and hydrophilic ILs when confined in hydrophilic nanopores. This structural change is associated with an up to 1 order-of-magnitude decrease in the effective viscosity. Screening of electrostatic interactions between anions and cations by water should make ILs more "fluid" and compressible, and thereby less viscous,[16] in agreement with our results. Electrostatic screening is only evidenced in the case of [EMIM][$EtSO_4$] through the prominent decrease in the screening length with the addition of water. Obviously, the water content in the nanoconfined hydrophobic ILs could be higher than in larger pores and in an unconfined state and justify a screening. However, water contents comparable to those in [EMIM][$EtSO_4$] would lead to phase separation in both [EMIM][FAP] and [EMIM]-[TFSI] under nanoconfinement, and therefore, it is not likely that screening of electrostatic interactions is a major factor in reducing the viscosity of these two ILs. Alternatively, water in ILs may also behave as a molecular solvent that hydrates (solvates) ions and competes with ions for space.[57] For instance, water can hydrogen bond with $[EMIM]^+$ in [EMIM][TFSI] and, thereby, favor ion-pair dissociation,[58] which is consistent with the decrease in effective viscosity. On the other hand, numerous NMR studies report that water in hydrophobic ILs may form its own network[59−61] and even facilitate ion association.[62] Our results do not provide any evidence that this happens, but it is evident that the decrease in viscosity induced by water is much less prominent for [EMIM][FAP], which is the most hydrophobic IL.

Another prominent electric and viscous effect is inferred from the stick length, D_s. Strong electrostatic interactions between the negatively charged surface and the cations, along with interionic interactions, lead to the immobilization of ∼2−3 anion−cation monolayers at the mica−liquid interface. Although we cannot directly probe the composition of the interface, the reduction of the stick length to ∼0 in equilibrium with the humid environment is consistent with the adsorption of water on the hydrophilic surface, which should contribute to the screening of electrostatic interactions at the interface and facilitate flow along the surface.[16] This is observed for both hydrophobic and hydrophilic ILs on mica in our experiments, and it can be expected for other hydrophilic surfaces, as well.

The results of this study support that water-in-IL electrolytes with modulated amounts of water that intercalate into the interfacial (layered) structure may enhance the fluidity of the electrolyte confined to hydrophilic nanopores and along hydrophilic surfaces. In hydrophilic ILs, the reduced viscosity by water stems from screening electrostatic interactions as well as solvation. Although water may accumulate at the electrolyte−electrode interface and undergo electrolysis,[18] recent MD simulations and electrochemical experiments propose that electrosorption of water is reduced when using hydrophilic ILs.[19] Interestingly, DFT theory also supports that the presence of trace amounts of impurities (like water) could enhance the energy density by modifying the charging mechanism, the origin of which is still under investigation.[63] Therefore, coupling hydrophilic ILs with water appears to be a promising pathway toward both safe and efficient operation of IL-based supercapacitors. Since water is ubiquitously present in the environment, the insights presented in this study will also help guide the design of IL-based systems for targeted applications and reduce their operational constraints in ambient environment.

5. CONCLUSIONS

This work investigated the influence of water on interfacial structure, dynamics, and electrostatic screening for three ILs confined between mica surfaces. In diffusion experiments, it

DOI: 10.1021/acsami.9b10923
ACS Appl. Mater. Interfaces 2019, 11, 33465−33477

was shown that surface-induced phase separation happened in the case of [EMIM][TFSI] above ~45% RH, due to both the high affinity of water to mica and the immiscibility between water and the IL. In contrast, [EMIM][$EtSO_4$], miscible at all ratios with water, remained in the pore despite the remarkable water uptake. The dynamic force measurements unveiled the change of the interfacial structure and dynamics induced by water. While water was intercalated within the IL films and affected the molecular packing, it did not disrupt layering. However, it decreased the effective viscosity by up to 1 order of magnitude compared to the dry ILs. By comparing the behavior of hydrophilic and hydrophobic ILs, the roles of water as dielectric medium that screens ionic charge and as a solvent that competes for space and disturbs ion packing were disentangled: while water may serve both roles in [EMIM]-[$EtSO_4$], the screening effect is not noticeable in the two hydrophobic ILs. Upon exposure to a humid environment, the presence of water reduced the stick length along the mica surface, which was associated with the screening of the electrostatic interactions between the negatively charged surface and the counterions. Considering that water promotes the flow of ILs through nanopores, and that hydrophilic ILs mitigate adsorption of water on electrode surfaces, as reported recently, water-in-(hydrophilic)ILs appear as promising electrolytes for next-generation IL-based supercapacitors.

■ ASSOCIATED CONTENT

Supporting Information

The Supporting Information is available free of charge on the ACS Publications website at DOI: 10.1021/acsami.9b10923.

Table with mean ion diameter, ion pair concentration, and dielectric constants of the ILs examined in the study; Table with the model parameters for eqs 1−8; Comparison of the effective viscosity of the three ILs at different humidity levels (PDF)

■ AUTHOR INFORMATION

Corresponding Author

*E-mail: rosae@illinois.edu.

ORCID

Rosa M. Espinosa-Marzal: 0000-0003-3442-2511

Author Contributions

The manuscript was written through contributions of all authors. All authors have given approval to the final version of the manuscript.

Notes

The authors declare no competing financial interest.

■ ACKNOWLEDGMENTS

This work was partially supported by the National Science Foundation Grant NSF CBET 19-16609.

■ REFERENCES

(1) Simon, P.; Gogotsi, Y.; Dunn, B. J. S. Where Do Batteries End and Supercapacitors Begin? *Science* **2014**, *343* (6176), 1210−1211.

(2) Simon, P.; Gogotsi, Y. Capacitive Energy Storage in Nanostructured Carbon-Electrolyte systems. *Acc. Chem. Res.* **2013**, *46* (5), 1094−1103.

(3) Béguin, F.; Presser, V.; Balducci, A.; Frackowiak, E. J. A. m. Carbons and Electrolytes for Advanced Supercapacitors. *Adv. Mater.* **2014**, *26* (14), 2219−2251.

(4) Armand, M.; Endres, F.; MacFarlane, D. R.; Ohno, H.; Scrosati, B. Ionic-liquid Materials for the Electrochemical Challenges of the Future. *Nat. Mater.* **2009**, *8* (8), 621−629.

(5) Hall, P. J.; Mirzaeian, M.; Fletcher, S. I.; Sillars, F. B.; Rennie, A. J. R.; Shitta-Bey, G. O.; Wilson, G.; Cruden, A.; Carter, R. Energy Storage in Electrochemical Capacitors: Designing Functional Materials to Improve Performance. *Energy Environ. Sci.* **2010**, *3* (9), 1238−1251.

(6) Wang, G.; Zhang, L.; Zhang, J. A Review of Electrode Materials for Electrochemical Supercapacitors. *Chem. Soc. Rev.* **2012**, *41* (2), 797−828.

(7) Osti, N. C.; Van Aken, K. L.; Thompson, M. W.; Tiet, F.; Jiang, D.-e.; Cummings, P. T.; Gogotsi, Y.; Mamontov, E. Solvent Polarity Governs Ion Interactions and Transport in a Solvated Room-temperature Ionic Liquid. *J. Phys. Chem. Lett.* **2017**, *8* (1), 167−171.

(8) Forse, A. C.; Griffin, J. M.; Merlet, C.; Carretero-Gonzalez, J.; Raji, A. R. O.; Trease, N. M.; Grey, C. P. Direct Observation of Ion Dynamics in Supercapacitor Electrodes Using In Situ Diffusion NMR Spectroscopy. *Nat. Energy* **2017**, *2* (3), 16216.

(9) Perkin, S. Ionic Liquids in Confined Geometries. *Phys. Chem. Chem. Phys.* **2012**, *14* (15), 5052−5062.

(10) Granick, S. Motions and Relaxations of Confined Liquids. *Science* **1991**, *253* (5026), 1374−1379.

(11) Han, M.; Espinosa-Marzal, R. M. Electroviscous Retardation of the Squeeze Out of Nanoconfined Ionic Liquids. *J. Phys. Chem. C* **2018**, *122* (37), 21344−21355.

(12) Kramer, G.; Hausen, F.; Bennewitz, R. Dynamic Shear Force Microscopy of Confined Liquids at a Gold Electrode. *Faraday Discuss.* **2017**, *199*, 299−309.

(13) Osti, N. C.; Van Aken, K. L.; Thompson, M. W.; Tiet, F.; Jiang, D. E.; Cummings, P. T.; Gogotsi, Y.; Mamontov, E. Solvent Polarity Governs Ion Interactions and Transport in a Solvated Room-Temperature Ionic Liquid. *J. Phys. Chem. Lett.* **2017**, *8* (1), 167−171.

(14) Espinosa-Marzal, R. M.; Arcifa, A.; Rossi, A.; Spencer, N. D. Microslips to "Avalanches" in Confined, Molecular Layers of Ionic Liquids. *J. Phys. Chem. Lett.* **2014**, *5* (1), 179−84.

(15) Espinosa-Marzal, R. M.; Arcifa, A.; Rossi, A.; Spencer, N. D. Ionic Liquids Confined in Hydrophilic Nanocontacts: Structure and Lubricity in the Presence of Water. *J. Phys. Chem. C* **2014**, *118* (12), 6491−6503.

(16) Fajardo, O. Y.; Bresme, F.; Kornyshev, A. A.; Urbakh, M. Water in Ionic Liquid Lubricants: Friend and Foe. *ACS Nano* **2017**, *11* (7), 6825−6831.

(17) Osti, N. C.; Dyatkin, B.; Thompson, M. W.; Tiet, F.; Zhang, P.; Dai, S.; Tyagi, M.; Cummings, P. T.; Gogotsi, Y.; Wesolowski, D. J.; Mamontov, E. Influence of Humidity on Performance and Microscopic Dynamics of an Ionic Liquid in Supercapacitor. *Phys. Rev. Materials* **2017**, *1* (3), 1 DOI: 10.1103/PhysRevMaterials.1.035402.

(18) Feng, G.; Jiang, X.; Qiao, R.; Kornyshev, A. A. Water in Ionic Liquids at Electrified Interfaces: The Anatomy of Electrosorption. *ACS Nano* **2014**, *8* (11), 11685−11694.

(19) Bi, S.; Wang, R.; Liu, S.; Yan, J.; Mao, B.; Kornyshev, A. A.; Feng, G. Minimizing the Electrosorption of Water from Humid Ionic Liquids on Electrodes. *Nat. Commun.* **2018**, *9* (1), 5222.

(20) Heuberger, M. The Extended Surface Forces Apparatus. Part I. Fast Spectral Correlation Interferometry. *Rev. Sci. Instrum.* **2001**, *72* (3), 1700−1707.

(21) Greenspan, L. Humidity Fixed Points of Binary Saturated Aqueous Solutions. *J. Res. Natl. Bur Stand* **1977**, *81* (1), 89−96.

(22) Gebbie, M. A.; Valtiner, M.; Banquy, X.; Fox, E. T.; Henderson, W. A.; Israelachvili, J. N. Ionic Liquids Behave as Dilute Electrolyte Solutions. *Proc. Natl. Acad. Sci. U. S. A.* **2013**, *110* (24), 9674−9679.

(23) Dzyaloshinskii, I. E.; Lifshitz, E. M.; Pitaevskii, L. P.; Priestley, M. The General Theory of Van der Waals Forces. In *Perspectives in Theoretical Physics*; Elsevier: 1992; pp 443−492.

(24) Horn, R. G.; Evans, D. F.; Ninham, B. W. Double-Layer and Solvation Forces Measured in a Molten-Salt and Its Mixtures with Water. *J. Phys. Chem.* **1988**, *92* (12), 3531−3537.

(25) Chan, D. Y. C.; Horn, R. G. The Drainage of Thin Liquid-Films between Solid-Surfaces. *J. Chem. Phys.* **1985**, *83* (10), 5311−5324.
(26) Bergman, D. J. The Dielectric Constant of a Composite Material—a Problem in Classical Physics. *Phys. Rep.* **1978**, *43* (9), 377−407.
(27) Tariq, M.; Carvalho, P. J.; Coutinho, J. A.; Marrucho, I. M.; Lopes, J. N. C.; Rebelo, L. P. Viscosity of (C2−C14) 1-Alkyl-3-methylimidazolium Bis (trifluoromethylsulfonyl) Amide Ionic Liquids in an Extended Temperature Range. *Fluid Phase Equilib.* **2011**, *301* (1), 22−32.
(28) Nazet, A.; Sokolov, S.; Sonnleitner, T.; Makino, T.; Kanakubo, M.; Buchner, R. Densities, Viscosities, and Conductivities of the Imidazolium Ionic Liquids [Emim][Ac], [Emim][FAP], [Bmim]-[BETI], [Bmim][FSI], [Hmim][TFSI], and [Omim][TFSI]. *J. Chem. Eng. Data* **2015**, *60* (8), 2400−2411.
(29) Torrecilla, J. S.; Rafione, T.; Garcia, J.; Rodriguez, F. Effect of Relative Humidity of Air on Density, Apparent Molar Volume, Viscosity, Surface Tension, and Water content of 1-ethyl-3-methylimidazolium Ethylsulfate Ionic Liquid. *J. Chem. Eng. Data* **2008**, *53* (4), 923−928.
(30) Raviv, U.; Frey, J.; Sak, R.; Laurat, P.; Tadmor, R.; Klein, J. Properties and Interactions of Physigrafted End-functionalized Poly(ethylene glycol) layers. *Langmuir* **2002**, *18* (20), 7482−7495.
(31) Zhang, Q. G.; Wang, N. N.; Yu, Z. W. The Hydrogen Bonding Interactions between the Ionic Liquid 1-ethyl-3-methylimidazolium Ethyl Sulfate and Water. *J. Phys. Chem. B* **2010**, *114* (14), 4747−4754.
(32) Fisher, L. R.; Israelachvili, J. N. Experimental Studies on the Applicability of the Kelvin Equation to Highly Curved Concave Menisci. *J. Colloid Interface Sci.* **1981**, *80* (2), 528−541.
(33) Christenson, H. K.; Horn, R. G.; Israelachvili, J. N. Measurement of Forces Due to Structure in Hydrocarbon Liquids. *J. Colloid Interface Sci.* **1982**, *88* (1), 79−88.
(34) Gardas, R. L.; Ge, R.; Ab Manan, N.; Rooney, D. W.; Hardacre, C. Interfacial Tensions of Imidazolium-based Ionic Liquids with Water and n-alkanes. *Fluid Phase Equilib.* **2010**, *294* (1−2), 139−147.
(35) Christenson, H. K.; Fang, J.; Israelachvili, J. N. Experimental Study of Phase Separation in Films of Molecular Dimensions. *Phys. Rev. B: Condens. Matter Mater. Phys.* **1989**, *39* (16), 11750−11754.
(36) Christenson, H. K.; Blom, C. E. Solvation Forces and Phase-Separation of Water in a Thin-Film of Nonpolar Liquid between Mica Surfaces. *J. Chem. Phys.* **1987**, *86* (1), 419−424.
(37) Cheng, H. W.; Dienemann, J. N.; Stock, P.; Merola, C.; Chen, Y. J.; Valtiner, M. The Effect of Water and Confinement on Self-Assembly of Imidazolium Based Ionic Liquids at Mica Interfaces. *Sci. Rep-Uk* **2016**, *6*, 30058.
(38) Perkin, S.; Albrecht, T.; Klein, J. Layering and Shear Properties of an Ionic Liquid, 1-ethyl-3-methylimidazolium Ethylsulfate, Confined to Nano-films between Mica Surfaces. *Phys. Chem. Chem. Phys.* **2010**, *12* (6), 1243−1247.
(39) Atkin, R.; Warr, G. G. Structure in Confined Room-Temperature Ionic Liquids. *J. Phys. Chem. C* **2007**, *111* (13), 5162−5168.
(40) Cheng, H. W.; Stock, P.; Moeremans, B.; Baimpos, T.; Banquy, X.; Renner, F. U.; Valtiner, M. Characterizing the Influence of Water on Charging and Layering at Electrified Ionic-Liquid/Solid Interfaces. *Adv. Mater. Interfaces* **2015**, *2* (12), 1500159.
(41) Sakai, K.; Okada, K.; Uka, A.; Misono, T.; Endo, T.; Sasaki, S.; Abe, M.; Sakai, H. Effects of Water on Solvation Layers of Imidazolium-Type Room Temperature Ionic Liquids on Silica and Mica. *Langmuir* **2015**, *31* (22), 6085−6091.
(42) Wang, Z.; Li, H.; Atkin, R.; Priest, C. Influence of Water on the Interfacial Nanostructure and Wetting of [Rmim][NTf2] Ionic Liquids at Mica Surfaces. *Langmuir* **2016**, *32* (35), 8818−8825.
(43) Jurado, L. A.; Kim, H.; Rossi, A.; Arcifa, A.; Schuh, J. K.; Spencer, N. D.; Leal, C.; Ewoldt, R. H.; Espinosa-Marzal, R. M. Effect of the Environmental Humidity on the Bulk, Interfacial and Nanoconfined Properties of an Ionic Liquid. *Phys. Chem. Chem. Phys.* **2016**, *18* (32), 22719−22730.
(44) Qiao, R. Water at Ionic Liquids-solid Interfaces. *Curr. Opin Electroche* **2019**, *13*, 11−17.
(45) Fedorov, M. V.; Kornyshev, A. A. Ionic Liquids at Electrified Interfaces. *Chem. Rev.* **2014**, *114* (5), 2978−3036.
(46) Feng, G.; Chen, M.; Bi, S.; Goodwin, Z. A. H.; Postnikov, E. B.; Brilliantov, N.; Urbakh, M.; Kornyshev, A. A. Free and Bound States of Ions in Ionic Liquids, Conductivity, and Underscreening Paradox. *Phys. Rev. X* **2019**, *9* (2), No. 021024.
(47) Lee, A. A.; Perez-Martinez, C. S.; Smith, A. M.; Perkin, S. Scaling Analysis of the Screening Length in Concentrated Electrolytes. *Phys. Rev. Lett.* **2017**, *119* (2), No. 026002.
(48) Smith, A. M.; Lee, A. A.; Perkin, S. The Electrostatic Screening Length in Concentrated Electrolytes Increases with Concentration. *J. Phys. Chem. Lett.* **2016**, *7* (12), 2157−2163.
(49) Bureau, L. Rate Effects on Layering of a Confined Linear Alkane. *Phys. Rev. Lett.* **2007**, *99* (22), 225503.
(50) Tomita, K.; Mizukami, M.; Nakano, S.; Ohta, N.; Yagi, N.; Kurihara, K. X-Ray Diffraction and Resonance Shear Measurement of Nano-Confined Ionic Liquids. *Phys. Chem. Chem. Phys.* **2018**, *20* (20), 13714−13721.
(51) Lee, A. A.; Perez-Martinez, C. S.; Smith, A. M.; Perkin, S. Underscreening in Concentrated Electrolytes. *Faraday Discuss.* **2017**, *199* (0), 239−259.
(52) Singh, T.; Kumar, A. Static Dielectric Constant of Room Temperature Ionic Liquids: Internal Pressure and Cohesive Energy Density Approach. *J. Phys. Chem. B* **2008**, *112* (41), 12968−12972.
(53) Levine, S.; Marriott, J. R.; Neale, G.; Epstein, N. Theory of Electrokinetic Flow in Fine Cylindrical Capillaries at High Zeta-Potentials. *J. Colloid Interface Sci.* **1975**, *52* (1), 136−149.
(54) Bureau, L. Nonlinear Rheology of a Nanoconfined Simple Fluid. *Phys. Rev. Lett.* **2010**, *104* (21), 218302.
(55) Ma, J.; Li, K.; Li, Z.; Qiu, Y.; Si, W.; Ge, Y.; Sha, J.; Liu, L.; Xie, X.; Yi, H.; Ni, Z.; Li, D.; Chen, Y. Drastically Reduced Ion Mobility in a Nanopore Due to Enhanced Pairing and Collisions between Dehydrated Ions. *J. Am. Chem. Soc.* **2019**, *141* (10), 4264−4272.
(56) Huang, J. Confinement Induced Dilution: Electrostatic Screening Length Anomaly in Concentrated Electrolytes in Confined Space. *J. Phys. Chem. C* **2018**, *122* (6), 3428−3433.
(57) Zhang, F.; Fang, C.; Qiao, R. Effects of Water on Mica-Ionic Liquid Interfaces. *J. Phys. Chem. C* **2018**, *122* (16), 9035−9045.
(58) Han, M.; Espinosa-Marzal, R. M. Strong Stretching of Poly(ethylene glycol) Brushes Mediated by Ionic Liquid Solvation. *J. Phys. Chem. Lett.* **2017**, *8* (17), 3954−3960.
(59) Rollet, A. L.; Porion, P.; Vaultier, M.; Billard, I.; Deschamps, M.; Bessada, C.; Jouvensal, L. Anomalous Diffusion of Water in [BMIM][TFSI] Room-temperature Ionic Liquid. *J. Phys. Chem. B* **2007**, *111* (41), 11888−11891.
(60) Fadeeva, T. A.; Husson, P.; DeVine, J. A.; Costa Gomes, M. F.; Greenbaum, S. G.; Castner, E. W., Jr. Interactions Between Water and 1-butyl-1-methylpyrrolidinium Ionic Liquids. *J. Chem. Phys.* **2015**, *143* (6), No. 064503.
(61) Cascao, J.; Silva, W.; Ferreira, A. S. D.; Cabrita, E. J. Ion Pair and Solvation Dynamics of [Bmim][BF4] + Water System. *Magn. Reson. Chem.* **2018**, *56* (2), 127−139.
(62) Yee, P.; Shah, J. K.; Maginn, E. J. State of Hydrophobic and Hydrophilic Ionic Liquids in Aqueous Solutions: Are the Ions Fully Dissociated? *J. Phys. Chem. B* **2013**, *117* (41), 12556−12566.
(63) Lian, C.; Liu, K.; Liu, H. L.; Wu, J. Z. Impurity Effects on Charging Mechanism and Energy Storage of Nanoporous Supercapacitors. *J. Phys. Chem. C* **2017**, *121* (26), 14066−14072.

DOI: 10.1021/acsami.9b10923
ACS Appl. Mater. Interfaces 2019, 11, 33465−33477